

Effect of Interhemispheric Field-Aligned Currents on Region-1 Currents

Sonya Lyatskaya^{1,3}, Wladislaw Lyatsky^{2,3}, and George V. Khazanov³,

¹ Howard Community College, Columbia, MD;

² Catholic University of America, Washington, DC;

³ NASA Goddard Space Flight Center, Greenbelt, MD

8 **Key Points**

9 Region1 can be a sum of current flowing from/to solar wind & interhemispheric current.

10 Interhemispheric currents can be related to "double auroral oval".

11 Accounting for interhemispheric currents can help predict Region1 features.

12

Abstract

An asymmetry in ionospheric conductivity between two hemispheres results in the formation of additional, interhemispheric field-aligned currents flowing between conjugate ionospheres within two auroral zones. These interhemispheric currents are especially significant during summer-winter conditions when there is a significant asymmetry in ionospheric conductivity in two hemispheres. In such conditions, these currents may be comparable in magnitude with the Region 1 field-aligned currents. In this case, the R1 current is the sum of two FACs: one is going from/to the solar wind, and another is flowing between conjugate ionospheres. These interhemispheric currents can also cause the formation of auroras extended along the nightside polar cap boundary, which may be related to the so-called “double auroral oval”. In this study, we present the results of analytical and numerical solutions for the interhemispheric currents and their effect on the Region 1 currents.

26 **Index Terms**

27 2721, 2431, 2736, 2753, 2784

28 **Key Words**

29 Field-aligned currents; Magnetosphere-ionosphere coupling; Region 1 current; High latitude

30 ionosphere; Interhemispheric currents

31

1. Introduction

There are three major systems of Field-Aligned Currents (FACs), transporting energy into and out from polar ionospheres: the R1 FACs at the polar cap boundary, the Region 2 (R2) FACs at the auroral zone equatorward boundary (both were extensively studied from observational data [e.g., *Iijima and Potemra*, 1976, 1978; *Weimer*, 2001; *Christiansen et al.*, 2002; *Papitashvili et al.*, 2002; *Anderson et al.*, 2005] and theoretically [e.g., *Jaggi and Wolf*, 1973; *Wolf*, 1975; *Harel et al.*, 1981; *Lyatsky and Maltsev*, 1983; *Spiro and Wolf*, 1984; *Richmond*, 1992; *Potemra*, 1994]), and the so-called “substorm current wedge” appearing during substorms [e.g., *McPherron et al.*, 1973].

More recent studies [*Benkevich et al.*, 2000; *Benkevich and Lyatsky*, 2000; *Ohtani et al.*, 2005a; 2005b; *Østgaard et al.*, 2005; *Lyatskaya et al.*, 2008, 2009; etc.] showed that an important role in the global 3-D current system can be played by the interhemispheric currents (IHCs). The IHCs redistribute ionospheric currents between two polar ionospheres in the regions of closed magnetic field lines in case of asymmetry of ionospheric conductivity between two polar ionospheres, which may happen during unequal illumination of polar ionospheres and other effects [e.g., *Richmond and Roble*, 1987; *Kozlovsky et al.*, 2003; *Atkinson and Hutchinson*, 1978; *Rishbeth*, 1997; *Benkevich et al.*, 2000; *Benkevich and Lyatsky*, 2000; *Yamashita and Iyemori*, 2002; *Lyatskaya et al.*, 2008; 2009; *Ohtani et al.*, 2005a, 2005b; *Østgaard et al.*, 2005, and references therein]. However, since it is difficult to separate the IHCs from other FACs (especially when they flow in the same region), despite the important role of the IHCs in dynamics of the global 3-D current system, they have not been sufficiently investigated.

The IHCs can be generated on the gradient of ionospheric conductivity (e.g., at the terminator separating the sunlit and dark ionospheric regions) and at the boundaries of auroral

precipitation regions. *Rishbeth* [1997] suggested that IHCs may be “a significant fraction of the total current, circulating in the ionosphere”, and the results of numerical modeling by *Benkevich et al.* [2000] showed that the IHCs can reach up to half of the R1 currents.

The IHCs can also affect the high-latitude ionosphere and upper atmosphere. The Joule heating by field-aligned and ionospheric currents are the main factor, which affects the temperature and expansion of the high-latitude ionosphere and upper atmosphere [e.g., *Chun et al.*, 2002; *Baker et al.*, 2004; *Knipp et al.*, 2005; *McHarg et al.*, 2005]. The present research and modeling results show that the role of IHCs is even more extensive than we suggested in our previous works.

The main purpose of this study is to examine the effect of interhemispheric FACs (IHCs) (which are flowing between two conjugate ionospheres) on the R1 FACs, which transport the electric field and energy from the solar wind to the ionosphere. The IHCs are especially significant during summer-winter conditions when there is significant asymmetry in ionospheric conductivity in two hemispheres; in these cases, the IHCs may be comparable in magnitude with and significantly affect the R1 currents. Another goal is to investigate a possible effect of the IHCs on the auroral events in the vicinity of the polar cap boundary such as the double auroral oval. These two problems are not investigated yet due to the necessity to solve this problem simultaneously in two hemispheres with different distributions of ionospheric conductivity.

2. Interhemispheric Currents near Polar Cap Boundary

For better understanding of the effect of IHCs on the R1 currents, first we consider a simple case when the polar cap and auroral zone have the shape of a circle and axisymmetric ring, respectively. The ionospheric conductivity poleward of the auroral equatorward boundary

in each hemisphere is assumed to be uniform. We also assume that the electric potential, φ_1 , coming from the magnetopause, is the same at both polar cap boundaries and varying as

$$\varphi_1 = E_0 r \sin \lambda, \quad (1)$$

where E_0 is the electric field (which we assume to be homogeneous and the same in both polar caps), and the angle, λ , is the longitude ($\lambda=0$ at the midnight meridian). The potential at the equatorward boundaries of the auroral zones is assumed to be zero due to the shielding effect on the plasma sheet inner boundary [e.g., *Jaggi and Wolf*, 1973], which is related to auroral zone equatorward boundaries. In this case, the potential in the auroral zone, φ_A , is a simple function of the radius, r , and the angle, λ ,

$$\varphi_A = E_0 \frac{r_{PC}^2}{r} \sin \lambda, \quad (2)$$

where r_{PC} is the polar cap radius. The potential and electric field distribution is the same in both hemispheres. The FACs are derived as $\nabla \cdot \mathbf{J}_i$, where \mathbf{J}_i are the ionospheric currents, $\mathbf{J}_i = \Sigma \mathbf{E}$, where Σ is the height-integrated ionospheric conductivity, and \mathbf{E} is the electric field. The obtained distribution of the FACs is schematically shown in Figure 1a. If conductivity distributions in two hemispheres are the same, the FACs distributions are also the same.

Then we consider a case when the ionospheric conductivity in two auroral zones is uniform but different in two hemispheres. In this case, we can expect that a part of ionospheric currents in one hemisphere can go along the highly-conductive magnetic field lines from one ionosphere to be closed in the opposite ionosphere, which results in the formation of the IHCs. The distribution of ionospheric currents and IHCs, I_{ih} , in this case is shown schematically in Figure 1b.

In the case of symmetric ionospheric conductivity in two hemispheres (as in Fig. 1a), the R1 currents (I_{R1}) on the polar cap boundaries correspond to the traditional R1 currents, equal to the I_{sw} currents going from and to the solar wind (these currents are generated near the magnetopause due to solar wind - magnetosphere dynamo effect). In this case, $I_{R1} = I_{sw}$. However, in the case of different ionospheric conductivities in two hemispheres (as in Fig. 1b), the FACs at the polar cap boundaries are the sum of two FACs: the traditional R1 currents (I_{sw}) going from/to the solar wind, and the IHCs (I_{ih})

$$I_{R1} = I_{sw} + I_{ih}, \quad (3)$$

Since both I_{sw} and I_{ih} currents in Figure 1b flow at the polar cap boundary, it is difficult to separate the I_{ih} from I_{sw} . To separate these currents, in the winter auroral zone we included a narrow conductive ring attached to the polar cap boundary (see Figure 2) with ionospheric conductivity equal to the conductivity in the conjugate region in the opposite summer ionosphere. Due to the small width of the ring, it insignificantly affects the magnitude of the currents; however, it relocates the I_{ih} currents to the equatorward boundaries of this ring, which allows separating the I_{sw} and I_{ih} currents. Note that a similar meridional displacement of I_{ih} currents relatively to I_{sw} at the night side in reality can be caused by the equatorward $\mathbf{E} \times \mathbf{B}$ convection drift of magnetospheric plasma across the polar caps, which results in the equatorward displacement of the I_{ih} FACs while they propagate between two hemispheres; this effect is known as the Alfvén wings (e.g., *Lyatsky et al.* [2010a]). The resulting equatorward displacement, Δr , of I_{ih} relatively to the polar cap boundary can be estimated on the ionospheric level as $\Delta r \approx V_d \Delta t$, where V_d is the equatorward $\mathbf{E} \times \mathbf{B}$ convection velocity, and Δt is the propagation time of the Alfvén wave, transporting FACs between two hemispheres (e.g., *Kivelson and Ridley* [2007]; *Lyatsky et al.* [2010b]). For reasonable values of $V_d \approx 0.3$ km/s and

122 $\Delta t \approx 5 \text{ min}$ ($\Delta t \approx l / V_A$ where l is the length of the field line and V_A is an average Alfven velocity
 123 along this field line), we obtain $\Delta r \approx 100 \text{ km}$ at the ionosphere level, which is sufficient for
 124 separation of these two currents. For simplicity, we assume that the equatorward displacement of
 125 the I_{ih} currents is the same for all local times; in this case, the problem is similar to that
 126 (considered above) with a narrow conductive ring attached to the polar cap boundaries in the
 127 winter ionosphere.

128 The resulting model is shown in Figure 2. The conductivity of the summer hemisphere
 129 (which is not shown) is high and uniform; the conductivity of the winter hemisphere is low and
 130 uniform everywhere except the narrow ring with conductivity equal to the conductivity in the
 131 conjugate summer ionosphere, which provides the separation between the I_{sw} and I_{ih} currents.
 132 This model also allows us to compare the results of analytical solution with numerical simulation
 133 (we remind that the results obtained in this case are related to the night side only).

134 In each hemisphere, there are three given regions: (1) the polar cap with the radius r_1 , (2)
 135 an adjacent narrow ring (shown in white on Fig.2 with the outer radius r_2 , and (3) the remaining
 136 auroral zone with outer radius r_3 . For simplicity, we suggest the Pedersen conductivity, Σ_P , to be
 137 equal to the Hall conductivity, Σ_H , in each of the regions (which is approximately correct in the
 138 case of relatively-low geomagnetic activity). In the entire Southern auroral zone, the conductivity
 139 is uniform, $\Sigma_P = \Sigma_H = 3S$, while in the Northern conductivity in the region 1 and 3: $\Sigma_{P1} = \Sigma_{H1} = \Sigma_{P3}$
 140 $= \Sigma_{H3} = 1S$, while in the region 2 (where $r_1 < r < r_2$) $\Sigma_{P2} = \Sigma_{H2} = 3S$. For calculating the potential
 141 distribution outside the polar caps, we solved the problem accounting for different conductivities
 142 in two auroral zones. Inside the polar caps, where the conductivities are different but uniform in
 143 each polar cap, the potential does not depend on conductivity and is derived by Eq. (1).

First, we computed the potential distribution, which is the same in both hemispheres due to high conductivity along the field lines. The analytical solution for the potential in three consecutive axially symmetric regions with accounting for both Pedersen and Hall conductivities can be written in the following form [Lyatsky and Maltsev, 1983; Lyatsky et al., 2006]:

$$\varphi_2 = E_0 \left[r_1 \frac{r/r_2 - r_2/r}{r_1/r_2 - r_2/r_1} \sin \lambda + \alpha r_2 \frac{r_1/r - r/r_1}{r_1/r_2 - r_2/r_1} \sin(\lambda - \lambda') \right] \quad (4)$$

$$\varphi_3 = E_0 \alpha r_2 \frac{r/r_3 - r_3/r}{r_2/r_3 - r_3/r_2} \sin(\lambda - \lambda') \quad (5)$$

where E_0 is the electric field within the polar cap, r_1 is the radius of a polar cap boundary (region 1 in the Fig. 2), r_2 and r_3 are the radii of the outer boundaries of the narrow ring (region 2) and the auroral zone (region 3), respectively, while φ_2 and φ_3 are potentials at the boundaries of these regions. The potential on the polar cap boundary is given by Eq. (1), the potential at the auroral zone equatorward boundary is assumed to be zero.

The coefficient α and the angle λ' in Eqs. (4, 5) are the functions of the radii and the Pedersen and Hall ionospheric conductivities of these zones:

$$\tan \lambda' = \frac{\Sigma_{H2} - \Sigma_{H3}}{\chi_2 \Sigma_{P2} + \chi_3 \Sigma_{P3}}; \quad -\frac{\pi}{2} < \lambda' < \frac{\pi}{2} \quad (6)$$

$$\alpha = \chi_1 \Sigma_{P2} \left[(\chi_2 \Sigma_{P2} + \chi_3 \Sigma_{P3})^2 + (\Sigma_{H2} - \Sigma_{H3})^2 \right]^{-1/2} \quad (7)$$

$$\chi_1 = \frac{2r_1^2}{r_2^2 - r_1^2}; \quad \chi_2 = \frac{r_2^2 + r_1^2}{r_2^2 - r_1^2}; \quad \chi_3 = \frac{r_3^2 + r_2^2}{r_3^2 - r_2^2} \quad (8)$$

Note that Lyatsky and Maltsev [1983] considered only the case of symmetric distributions of ionospheric conductivity in two hemispheres, and they did not account for IHCs. In the case of different ionospheric conductivity in two hemispheres and the existence of IHCs, we should assume the conductivities in the regions 2 and 3 to be the sums of the related ionospheric

conductivities in Northern and Southern auroral zones. The FACs (including the IHCs) are found from the computed electric field in each of these regions. Then we used our numerical model that includes IHCs [Benkevich *et al.*, 2000] for the same conductivity distribution. The obtained results were compared and found very close. For the potential difference across the polar caps of 100 KV, we obtained the following magnitudes of the currents in Northern hemisphere: $I_{R1}=0.46$ MA, $I_{ih}=0.19$ MA, $I_{R2}=0.14$ MA; and in Southern hemisphere: $I_{R1}=0.66$ MA, $I_{ih}=0.19$ MA, $I_{R2}=0.42$ MA. The computed distributions of the ionospheric and field-aligned currents are shown in Figure 3.

3. Discussion and Conclusion

In this study, we investigated the effect of the interhemispheric currents (IHCs) on the R1 FACs, which transport the electric field and energy from the solar wind into the ionosphere. In the case of asymmetry in ionospheric conductivity between two hemispheres (particularly, during summer-winter conditions and specific UT intervals), the R1 currents on the polar cap boundaries are significantly different from the traditional R1 FACs related to symmetric ionospheric conductivity in two hemispheres. In the case of interhemispheric asymmetry in ionospheric conductivity, the FACs on the polar cap boundary include also (additionally to the traditional R1 currents) the IHCs going along the closed magnetic field lines between two conjugate ionospheres. The magnitude of these IHCs is proportional to the difference in ionospheric conductivities in two hemispheres on the polar cap boundaries, and during summer-winter seasons the IHCs can be comparable in magnitude with the R1 FACs. This shows the important contributions from the IHCs to the global current system.

Accounting for the $\mathbf{E} \times \mathbf{B}$ convection drift of magnetospheric plasma with the frozen-in magnetic field results in an equatorward displacement of the IHCs on the night side (while these currents propagate between two hemispheres). This displacement of the IHCs relatively to the polar cap boundary results in the formation of double-stream FACs near the nightside polar cap boundary. As a result, the two FACs, separated along the meridian, in summer hemisphere have the same direction, whereas in the winter hemisphere these currents flow in opposite directions. The spatial separation of the FACs near the polar cap boundary can partially explain the separation of FACs near the polar cap boundary, observed with the ST-5 spacecraft [e.g., *Le et al.*, 2008, 2009].

In the winter hemisphere, the spatially-separated double-stream FACs flow in opposite directions; these FACs can be responsible for the formation of the so-called “double auroral oval” [e.g., *Elphinstone et al.*, 1995; *Lyatsky et al.*, 2001; *Kornilova et al.*, 2006; *Ohtani et al.*, 2012]. Indeed, it is well known [e.g., *Knight*, 1973; *Janhunen and Olsson*, 1998] that the energy flux of precipitating electrons depends on the direction of FACs: to provide upward-directed FACs in heated plasma in the convergent magnetic field, it should be a field-aligned electric field accelerating these electrons. Thus, the upward FACs are associated with fluxes of accelerated precipitating electrons, which can result in increasing auroral activity. Since the double-stream FACs in winter hemisphere flow in opposite directions, one of these FACs (upward-directed) can be responsible for the generation of the auroras and the formation of auroras along the nightside polar cap boundary, which is the main feature of the double auroral oval. Note that this explanation for these events is only one of possible effect contributing to the double auroral oval configuration; other explanations were proposed, e.g., by *Ohtani et al.* [2012] and recently *Sandholt et al.* [2014].

Thus, in this study we showed that any asymmetry in solar luminosity and, consequently, ionospheric conductivity in two hemispheres results in the generation of the IHCs flowing between two hemispheres. These IHCs can significantly affect the global 3-D current system in winter/summer conditions and some UT intervals.

The main results of this study can be summarized are follows:

(1) Thus, in the case of asymmetry in ionospheric conductivity between two hemispheres, the R1 currents are the sum of two FACs: the traditional R1 FACs (the I_{sw} currents) going from/to the solar wind, and the interhemispheric currents (IHCs). In a sunlit hemisphere, the IHCs are going in the same direction as the I_{sw} currents, which results in increasing R1 currents. In the winter hemisphere, however, the IHCs are directed oppositely to the I_{sw} currents; as a result, the magnitude of the R1 currents in dark winter hemisphere can be less than each of these currents. In the case considered in this study, the IHCs in the winter hemisphere comprise approximately 40% of the total R1 currents. The strong contribution from the IHCs to the R1 currents explains an important role played by the IHCs in the dynamics of the total 3-D current system.

(2) Although both I_{sw} currents and IHCs are placed near the polar cap boundary (the boundary of open-closed field lines), the locations of these two currents do not totally coincide (at least at the night side) due to an equatorward displacement of the IHCs while they propagate to the opposite hemisphere. This equatorward displacement of the IHCs with respect to the I_{sw} currents results in the formation the double-stream FACs near the nightside polar cap boundaries.

(3) The formation of double-stream FACs near the nightside winter polar cap boundary can lead to some interesting results. Since upward FACs are usually associated with fluxes of accelerated electrons precipitating into the ionosphere (that is explained as a result of the Knight

mechanism [e.g., *Knight*, 1973]), the double-stream FACs over the nightside polar cap boundary can create a band of precipitating accelerated electrons and auroras stretched out along the polar cap boundary. In the evening sector, this band can be associated with the upward I_{sw} FACs (the traditional R1 FACs) while in the morning sector the upward-directed IHCs, located somewhat equatorward of the polar cap boundary, can be observed as part of so-called “double auroral oval” [e.g., *Elphinstone et al.*, 1995; *Lyatsky et al.*, 2001; *Kornilova et al.*, 2006; *Ohtani et al.*, 2012].

Acknowledgment

This study is supported by the National Science Foundation under Award No. ANT-1204019.

References

- Anderson, B. J., S.-I. Ohtani, H. Korth and A. Ukhorskiy (2005), Storm time dawn-dusk asymmetry of the large-scale Birkeland currents, *J. Geophys. Res.*, 110, A12220.
- Atkinson, G., and D. Hutchinson (1978), Effect of day-night ionospheric conductivity on polar cap convective flow, *J. Geophys. Res.*, 83, 725.
- Baker, J. B. H., Y. Zhang, R.A. Greenwald, L.J. Paxton, and D. Morrison (2004), Height-integrated Joule and auroral particle heating in the night side high latitude thermosphere, *Geophys. Res. Lett.*, 31, L09807.
- Benkevich, L., and W. Lyatsky (2000), Detached Vortices in Equivalent Ionospheric Currents in the Winter Dayside Ionosphere, *Geophys. Res. Lett.*, 27(9), 1375–1378.
- Benkevich, L., W. Lyatsky, and L. L. Cogger (2000), Field-aligned currents between conjugate hemispheres, *J. Geophys. Res.*, 105(A12), 27,727–27,737.

255 Christiansen, F., V. O. Papitashvili, and T. Neubert (2002), Seasonal variations of high-latitude
 256 field-aligned currents inferred from Ørsted and Magsat observations, *J. Geophys. Res.*,
 257 107(A2), 1029, doi:10.1029/2001JA900104.

258 Chun, F. K., D. J. Knipp, M. G. McHarg, et al. (2002), Joule heating patterns as a function of
 259 polar cap index, *J. Geophys. Res.*, 107(A7), 1119.

260 Elphinstone, R. D., J. S. Murphree, D. J. Hearn, et al.(1995), The double oval UV auroral
 261 distribution: 1. Implications for the mapping of auroral arcs, 100, A7, 12075–12092;
 262 DOI: 10.1029/95JA00326

263 Harel, M., R. A. Wolf, P. H. Reiff, R. W. Spiro, W. J. Burke, F. J. Rich, and M. Smiddy (1981),
 264 Quantitative Simulation of A Magnetospheric Substorm, 1. Model Logic and Overview, *J.*
 265 *Geophys. Res.*, 86(A4), 2217–2241.

266 Iijima, T., and T. A. Potemra (1976), The amplitude distribution of field-aligned currents at
 267 northern high latitudes observed by TRIAD, *J. Geophys. Res.*, 81, 2165.

268 Iijima, T., and T. A. Potemra (1978), Large-scale characteristics of field-aligned currents
 269 associated with substorms, *J. Geophys. Res.*, 83, 599–615.

270 Jaggi, R. K., R. A. Wolf, (1973) Self-consistent calculation of the motion of a sheet of ions in the
 271 magnetosphere, *J. Geophys. Res.*, 78, 16, 2852–2866, 1973.

272 Janhunen, P., and A. Olsson (1998), The current-voltage relationship revisited: exact and
 273 approximate formulas with almost general validity for hot magnetospheric electrons for bi-
 274 Maxwellian and kappa distributions, *Ann. Geophys.*, 16, 292-297.

275 Knight, L., Parallel electric fields, *Planet. Space Sci.*, 21, 741, 1973.

276 Kivelson, M. G., and A. J. Ridley (2008), Saturation of the polar cap potential: Inference from
 277 Alfvén wing arguments, *J. Geophys. Res.*, 113, A05214, doi:10.1029/2007JA012302.

278 Knipp, D., W. Tobiska, and B. Emery (2005), Direct and Indirect Thermospheric Heating
 279 Sources for Solar Cycles 21–23, *Solar Physics*, 224, 1-2, 495-505.

280 Kornilova, T. A., I. A. Kornilov, O. I. Kornilov (2006), “Auroral intensification structure and
 281 dynamics in the double oval: Substorm of December 26, 2000”, *Geomagn. Aeronomy*, 46, 4,
 282 450-456.

283 Kozlovsky, A., T. Turunen, A. Koustov, and G. Parks (2003), IMF By effects in the
 284 magnetospheric convection on closed magnetic field lines, *Geophys. Res. Lett.*, 30(24), 2261.

285 Le, G., J. A., Slavin, and R. J. Strangeway (2008), Space Technology 5 observations of the
 286 imbalance of regions 1 and 2 field-aligned currents and its implication to the cross-polar cap
 287 Pedersen currents, *J. Geophys. Res.*, 115, No. A7, A07202.

288 Le, G., Y. Wang, J. A. Slavin, and R. J. Strangeway (2009), Space Technology 5 Multi-point
 289 observations of temporal and spatial variability of field-aligned currents, *J. Geophys. Res.*,
 290 114, A08206, doi:10.1029/2009JA014081.

291 Lyatskaya, S., W. Lyatsky, and G. V. Khazanov (2008), Relationship between Substorm Activity
 292 and Magnetic Disturbances in Two Polar Caps, *Geophys. Res. Lett.*, 35, L20104.

293 Lyatskaya, S., W. Lyatsky, G. V. Khazanov (2009), Auroral electrojet AL index and polar
 294 magnetic disturbances in two hemispheres, *J. Geophys. Res.*, 114, A06212.

295 Lyatsky, W. B., and Y. P. Maltsev (1983), *Magnetosphere-Ionosphere Interaction*, “Nauka”,
 296 Moscow.

297 Lyatsky, W., L. L. Cogger, B. Jackel, A. M. Hamza, W. J. Hughes, D. Murr, and Ole Rasmussen
 298 (2001), *J. Atmos. Sol.-Terr. Phys.*, 63, 1609–1621.

299 Lyatsky, W., A. Tan, and G. V. Khazanov (2006), A simple analytical model for subauroral
 300 polarization stream (SAPS), *Geophys. Res. Lett.*, 33, L19101, doi:10.1029/2006GL025949.

301 Lyatsky, W., G. V. Khazanov, and J. A. Slavin (2010a), Alfvén Wave Reflection model of field-
 302 aligned currents at Mercury, *Icarus*, 209, 40–45.

303 Lyatsky, W., G. V. Khazanov, and J. A. Slavin (2010b), Saturation of the electric field
 304 transmitted to the magnetosphere, *J. Geophys. Res.*, 115, A08221, doi:10.1029/2009JA015091.

305 McPherron, R. L., C. T. Russell, and M. Aubry (1973), Satellite studies of magnetospheric
 306 substorms on August 15, 1978, 9, Phenomenological model for substorms, *J. Geophys. Res.*,
 307 78, 3131-3149.

308 McHarg, M., F. Chun, D. Knipp, et al. (2005), High-latitude Joule heating response to IMF
 309 inputs, *J. Geophys. Res.*, 110, A08309; DOI: 10.1029/2004JA010949.

310 Ohtani, S., G. Ueno, and T. Higuchi (2005a), Comparison of large-scale field-aligned currents
 311 under sunlit and dark ionospheric conditions, *J. Geophys. Res.*, 110, A09230.

312 Ohtani, S., G. Ueno, T. Higuchi, and H. Kawano (2005b), Annual and semiannual variations of
 313 the location and intensity of large-scale field-aligned currents, *J. Geophys. Res.*, 110, A01216.

314 Ohtani, S., H. Korth, S. Wing, E. R. Talaat, H. U. Frey, and J. W. Gjerloev (2012), The Double
 315 Auroral Oval in the Dusk-to-Midnight Sector: Formation, Mapping and Dynamics, *J. Geophys.*
 316 *Res.*, 117, A08203, doi:10.1029/2011JA017501.

317 Østgaard, N., N. A. Tsyganenko, S. B. Mende, H. U. Frey, T. J. Immel, M. Fillingim, L. A.
 318 Frank, and J. B. Sigwarth (2005), Observations and model predictions of substorm auroral
 319 asymmetries in the conjugate hemispheres, *Geophys. Res. Lett.*, 32, L05111.

320 Papitashvili, V. O., F. Christiansen, and T. Neubert (2002), A new model of field-aligned
 321 currents derived from high-precision satellite magnetic field data, *Geophys. Res. Lett.*, 29,
 322 1683.

323 Potemra, T. A. (1994), Sources of large-scale Birkeland currents, in Physical Signatures of
 324 Magnetospheric Boundary Layer Processes, Ed. by J. A. Holtet and A. Egeland, p.3, Kluwer
 325 Academic Publishers.
 326 Richmond, A. D., and R. G. Roble (1987), Electrodynamics effects of thermospheric winds from
 327 NCAR thermospheric general circulation model, *J. Geophys. Res.*, 92, 12,365-12,376.
 328 Richmond, A. D. (1992), Assimilative mapping of ionospheric electrodynamics, *Adv. Space*
 329 *Res.*, 12(6), 59–68.
 330 Rishbeth, H. (1997), The ionospheric E-layer and F-layer dynamos - a tutorial review, *J. Atmos.*
 331 *Solar-Terr. Phys.*, 59 (15), 1873-1880.
 332 Sandholt, P. E., C. J. Farrugia, and W. F. Denig, M–I coupling across the auroral oval at dusk
 333 and midnight: repetitive substorm activity driven by interplanetary coronal mass ejections
 334 (CMEs), *Ann. Geophys.*, 32, 333–351, 2014; doi:10.5194/angeo-32-333-2014
 335 Spiro, R. W., R. A. Wolf (1984), Electrodynamics of convection in the inner magnetosphere, in:
 336 Potemra T. A. (Ed.), *Magnetospheric Currents, Geophys. Monogr. Ser.*, 28, 247–259.
 337 Weimer, D.R. (2001), Maps of ionospheric field-aligned currents as a function of the
 338 interplanetary magnetic field derived from Dynamics Explorer 2 data, *J. Geophys. Res.*, 106,
 339 12,889-12,902.
 340 Wolf, R. A. (1975), Ionosphere-Magnetosphere Coupling, *Space Sci. Rev.*, 17, 537-562.
 341 Yamashita, S., and T. Iyemori (2002), Seasonal and local time dependences of the
 342 interhemispheric field-aligned currents deduced from the Ørsted satellite and the ground
 343 geomagnetic observations, *J. Geophys. Res.*, 107 (A11), 1372.
 344

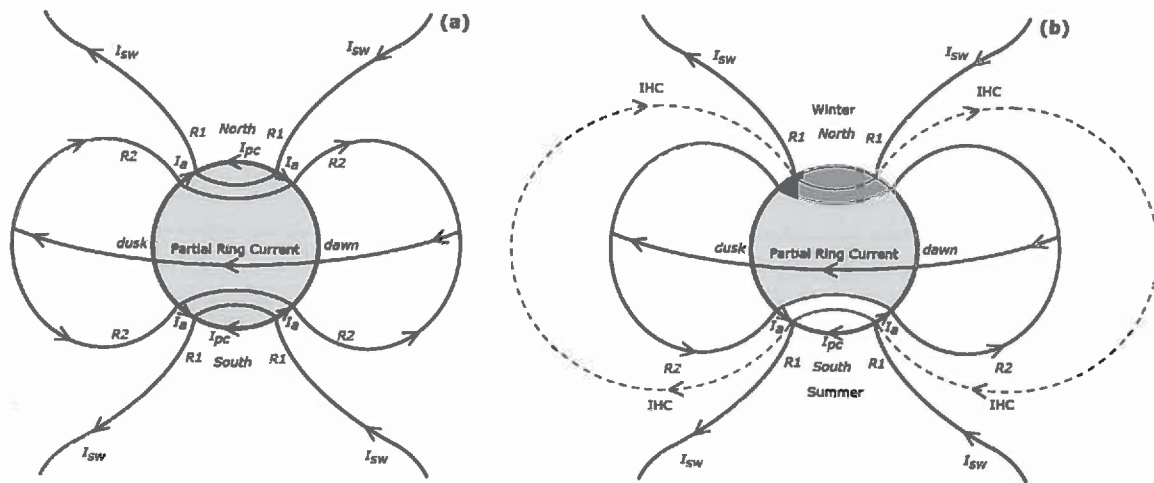


Figure 1. A sketch of FACs and ionospheric currents in the dawn-dusk meridional cross-section for the cases: (a) when the ionospheric conductivity is the same in both hemispheres and (b) when the conductivity in Southern high-latitude ionosphere is higher than that in the Northern hemisphere. In the first (a) case, the traditional R1 currents are going on the polar cap boundaries from and to the solar wind (these FACs closing through the solar wind we will call the I_{sw}), while in the case (b) the R1 currents are the sum of the I_{sw} and IHCs. Shown also are the R2 FACs closing the partial Ring Currents in the vicinity of the equatorial plane, and ionospheric currents in the polar caps, I_{pc} , and auroral zones, I_a . The ionospheric conductivity in Northern auroral zone and polar cap in Figure 1b is assumed to be very low.

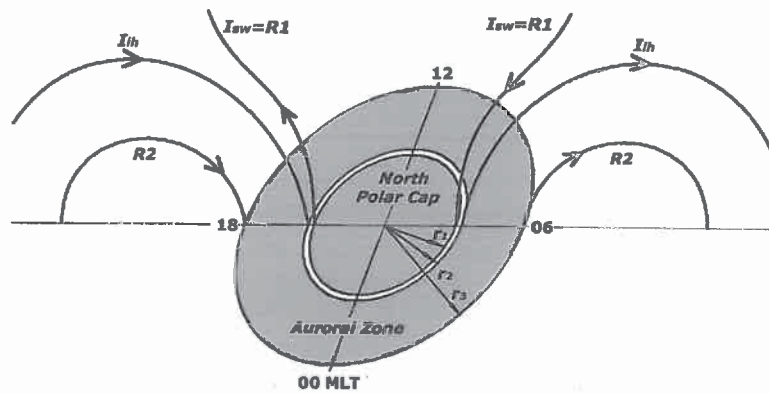
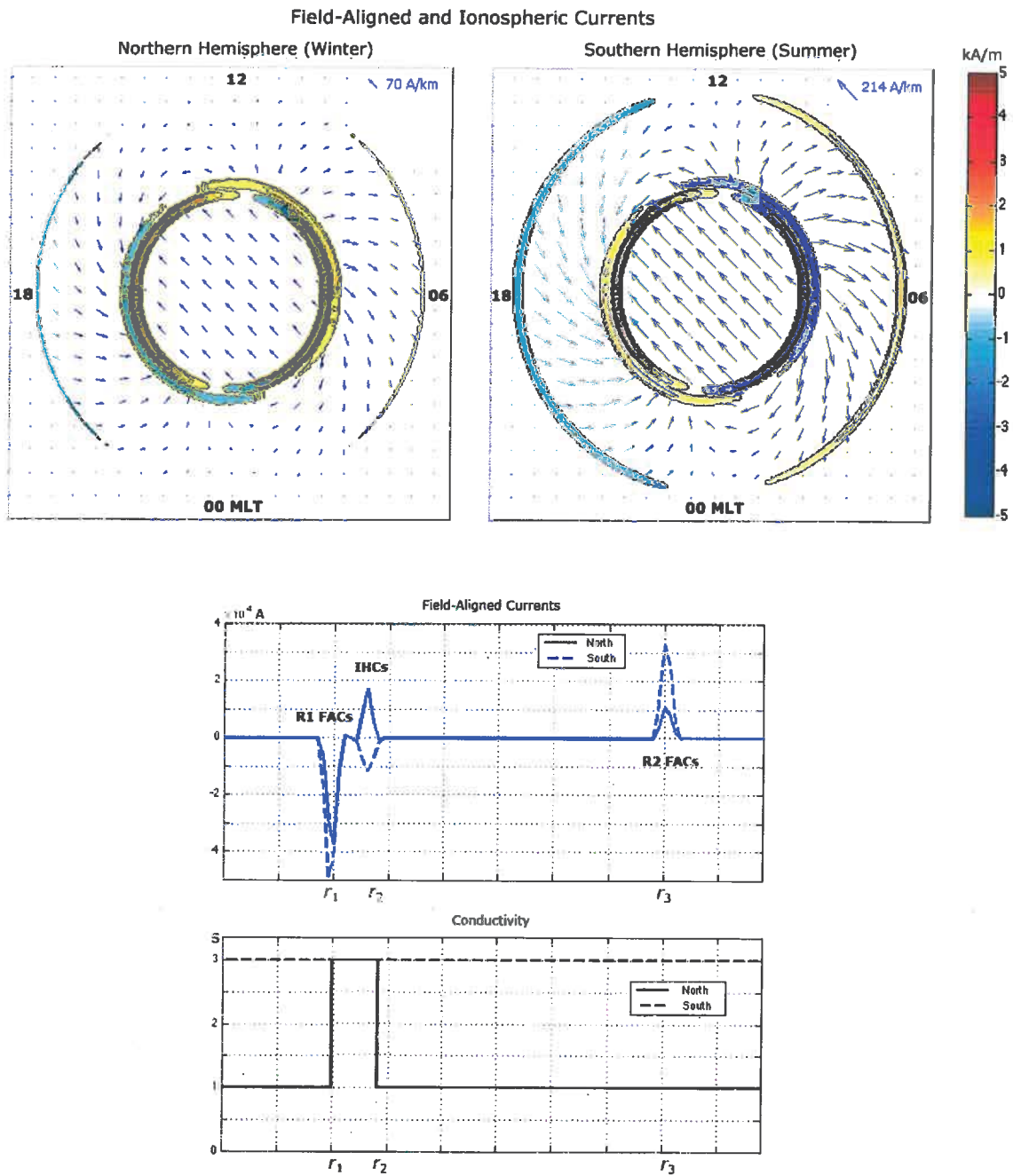


Figure 2. A sketch showing the solar wind I_{sw} currents (going from/to the solar wind) and separated interhemispheric I_{ih} currents (flowing at the outer boundary of the narrow ring of enhanced conductivity shown in white) in Northern winter hemisphere. The $R2$ currents at the auroral zone outer boundary are also shown. The ionospheric conductivity in the auroral zone is assumed to be much less than that in the opposite summer auroral zone. Note that in the case of separated I_{sw} and I_{ih} currents, the $R1$ currents are equal to solar wind currents $I_{R1} = I_{sw}$.



364

365 **Figure 3.** Computed currents in Northern winter hemisphere (top left) and Southern summer
 366 hemisphere (top right). Ionospheric currents are shown by blue arrows. The magnitude of FACs
 367 is shown as the contour plots. FACs entering the ionosphere are shown in blue while going out
 368 from in red and yellow. The FACs currents going from/to the solar wind at the polar cap

369 boundaries are shown as the I_{sw} currents, the FACs at the outer boundaries of the narrow rings
370 slightly equatorward of the polar caps are the interhemispheric currents (I_{ih}); the FACs at the
371 outer boundaries of the auroral zones are the R2 currents. Note that I_{ih} currents have the same
372 direction as the I_{sw} currents in summer hemisphere (the top right panel) but the opposite
373 directions in winter hemisphere (the top left panel). The panels below show the meridional plots
374 of the relative locations of the FACs, integrated within 20° of longitude along the dawn meridian
375 (06 MLT), and the conductivity profile (lower panel) in the same meridian. Currents and
376 conductivity in the Northern hemisphere are shown in solid, while in Southern in dashed lines.